Arteriosclerosis, Thrombosis, and Vascular Biology

BASIC SCIENCES

Whole-Body Knockout of the AhR (Aryl Hydrocarbon Receptor) Ameliorates Atherosclerosis Due to Altered Lipid Metabolism—Brief Report

Rosanna Huchzermeier,* Renske J. de Jong,* Leonida Rakateli, Andrea Bonnin-Marquez, Sanne L. Maas, Chantal Maassen-Pöttgens, Kathrin Abschlag, Han Jin, Anna-Lena Geiselhöringer, Vasiliki Triantafyllidou, Donato Santovito, Joachim Jankowski, Erik A.L. Biessen, Caspar Ohnmacht, Emiel P.C. van der Vorst

BACKGROUND: Atherosclerotic cardiovascular disease, characterized by an imbalanced lipid metabolism and a dysregulated immune response, is a major cause of death worldwide. The AhR (aryl hydrocarbon receptor) is a ligand-activated transcription factor that is highly expressed in the liver and primarily known for its role in detoxification. However, recent studies suggest that the AhR also plays a key role in immune regulation, indicating that this receptor can influence the development of atherosclerosis.

METHODS: *Apoe*$^{-/-}$ and *Apoe*$^{-/-}$*Ahr*$^{-/-}$ mice were fed a western-type diet for 12 weeks to induce atherosclerosis. Aortic roots were analyzed for size and composition of atherosclerotic plaques. Plasma samples were characterized for inflammation and lipid levels. Liver samples were analyzed for cytokines and lipid accumulation and subjected to RNA sequencing and kinomics. A PheWAS (Phenome-Wide Association Study) was performed to identify associations of genetic *AHR* variants with atherosclerotic cardiovascular disease and lipid phenotypes in humans.

RESULTS: The number of circulating leukocytes was increased in *Apoe*$^{-/-}$*Ahr*$^{-/-}$ mice compared with *Apoe*$^{-/-}$ controls. Surprisingly, however, mice lacking *Ahr* showed significantly smaller plaques than *Apoe*$^{-/-}$ mice, which coincided with strongly reduced plasma cholesterol and triglyceride levels. The liver lipid levels showed a similar effect, indicating a key role of the AhR in lipid metabolism. RNA sequencing of the liver revealed that lipid metabolism pathways were particularly impacted in *Apoe*$^{-/-}$*Ahr*$^{-/-}$ mice. Furthermore, through kinomics, we identified signaling pathways affected by the absence of *Ahr*. PheWAS analysis revealed significant associations between the *AHR* variant rs4410790 and lipid traits, including plasma triglycerides, LDL (low-density lipoprotein), and total cholesterol.

CONCLUSIONS: Our study demonstrates a remarkable role for AhR in the pathogenesis of atherosclerosis, interfering with both lipid metabolism and inflammatory pathways. Although the underlying mechanisms remain unclear, these results demonstrate a novel and crucial role for AhR in atherosclerotic cardiovascular disease.

GRAPHIC ABSTRACT: A graphic abstract is available for this article.

Key Words: atherosclerosis ■ cardiovascular diseases ■ lipid metabolism ■ mice, knockout ■ receptors, aryl hydrocarbon

Atherosclerotic cardiovascular disease is characterized by chronic inflammation and lipid accumulation in the vascular wall and remains one of the leading causes of mortality worldwide.[1] Treatment strategies that primarily target patients' lipid levels still do not provide sufficient efficacy and carry a high risk of side effects.[1] Therefore, further research into new potential therapeutic targets is indispensable.

Correspondence to: Emiel P.C. van der Vorst, PhD, Aachen-Maastricht Institute for Cardio-Renal Disease, Pauwelsstrasse 17, 52074 Aachen, Germany. Email evandervorst@ukaachen.de
*R. Huchzermeier and R.J. de Jong contributed equally.
Supplemental Material is available at https://www.ahajournals.org/doi/suppl/10.1161/ATVBAHA.125.323673.
For Sources of Funding and Disclosures, see page 617.

Arterioscler Thromb Vasc Biol is available at www.ahajournals.org/journal/atvb

Nonstandard Abbreviations and Acronyms

Acot11	acyl-coenzyme A thioesterase
AhR	aryl hydrocarbon receptor
ALT	alanine-amino-transferase
ARAF	A-Raf proto-oncogene, serine/threonine kinase
ARNT	aryl hydrocarbon receptor nuclear translocator
AST	aspartate aminotransferase
BRAF	B-Raf proto-oncogene, serine/threonine kinase
CCL2	CC-chemokine ligand 2
LDL	low-density lipoprotein
PheWAS	Phenome-Wide Association Study
RAF1	Raf-1 proto-oncogene, serine/threonine kinase
Socs3	suppressor of cytokine signaling
STK	serine-threonine kinase
TNF	tumor necrosis factor
Usp2	ubiquitin-specific peptidase

A key player in organ detoxification, a new mediator of inflammation, is the AhR (aryl hydrocarbon receptor), as recent studies suggest.[2] The AhR is a cytosolic transcription factor reacting to a variety of endogenous, for example, kynurenine, and exogenous ligands, such as 2,3,7,8-tetrachlorodibenzo-p-dioxin. Upon ligand binding, the protein dissociates from its cochaperones, enabling its translocation into the nucleus. By binding to the ARNT (AhR nuclear translocator), the AhR-ARNT complex binds to the xenobiotic response element and alters gene transcription of many target genes. The primary target gene is *Cyp1a1*. The activation of the AhR and the resulting gene transcription not only impact the detoxification but also cell processes such as cell proliferation and adhesion.[2] In addition, recent studies suggest that AhR plays a regulatory role in immune responses.[2] A study by Natividad et al[3] demonstrated that decreased AhR activity is associated with increased systemic inflammation. These findings indicate a potential protective role of the AhR in atherosclerotic cardiovascular disease.[4]

Therefore, we hypothesize that the absence of AhR in mice will lead to increased inflammation and, consequently, to the development of atherosclerotic plaque. In this study, multiorgan analyses were performed using whole-body AhR knockout mice on an atherogenic apolipoprotein E–deficient (*Apoe*$^{-/-}$) background to determine the influence of AhR on atherosclerosis formation, as well as the lipid and inflammatory status.

MATERIALS AND METHODS

The data that support the findings of this study are available from the corresponding author upon reasonable request.

What Are the Clinical Implications?

This study identifies the AhR (aryl hydrocarbon receptor) as a regulator of hepatic lipid metabolism, as *Ahr* deficiency reduced plasma cholesterol and triglyceride levels. Interestingly, the lack of *Ahr* unexpectedly limited atherosclerotic plaque formation in *Apoe*$^{-/-}$ mice despite leukocytosis, suggesting that the effects of lipids have a dominant impact on plaque development. Liver transcriptomics and kinase profiling implicate altered lipid biosynthesis/transport and highlight ApoA-IV upregulation as a potential mediator. Human genetic associations at the AhR locus (rs4410790) with coronary artery disease and lipid traits support translational relevance. Collectively, these findings motivate exploration of AhR-modulating therapies to reduce lipids and atherosclerosis, with careful attention to ligand specificity, sex differences, and safety, and raise opportunities for genetic stratification to personalize cardiovascular prevention.

Animals

Apoe$^{-/-}$*Ahr*$^{-/-}$ mice were generated by crossbreeding *Apoe*$^{-/-}$ mice with *Ahr*$^{-/-}$ mice (B6.129-Ahrtm1Bra/J, Jax strain number 00283136). Both males and females were used for all experiments. The mice were fed a high-fat diet (containing 21.1% crude fat, 17.3% crude protein, 5.0% crude fiber, 4.2% crude ash, 14.4% starch, 34.3% sugar, and 0.21% cholesterol; Sniff TD88137), starting at 8 weeks of age. After 12 weeks of high-fat diet feeding, the final euthanasia of the experimental animals is performed under deep, nonantagonizable anesthesia (10-mg/kg xylazine and 100-mg/kg ketamine) with subsequent blood collection by retro-orbital puncture using anticoagulant capillaries. Two independent experiments were conducted, each containing at least 4 males and females per genotype. All animal studies were approved by the local ethical committee (Regierung von Oberbayern, Germany, approval number ROB-55.2-2532.Vet 02-17-222 and Landesamt für Natur, Umwelt und Verbraucherschutz Nordrhein-Westfalen, Germany, approval number 81-02.04.2019.A363). All procedures are in accordance with the guidelines outlined in Directive 2010/63/EU of the European Parliament on the protection of animals used for scientific purposes.

Atherosclerotic Lesion Analysis

Hearts were fixated in 4% paraformaldehyde and embedded in Tissue-Tek O.C.T. compound (Sakura) for transverse cryosectioning. Aortic arches were fixed in 4% paraformaldehyde and embedded in paraffin afterwards for sectioning. Atherosclerotic plaque size was quantified using hematoxylin-eosin staining in the aortic roots (hematoxylin-eosin, Sigma). Masson trichrome staining for collagen deposition was performed on aortic roots to analyze collagen and necrotic core content. The macrophage infiltration was investigated by immunofluorescence costaining on aortic roots. Galectin 3 (Mac2) was stained after antigen retrieval by incubation in citrate buffer (anti-mouse Mac2 antibody, Cedarlane). After blocking the unspecific binding sites with PBS (0.01% BSA, 0.0125% horse serum), the Mac2 antibody, diluted in PBS (0.015% of the blocking solution),

was incubated overnight at 4 °C. Secondary antibody DL488 was incubated for 1 hour at room temperature, diluted in PBS (0.015% blocking solution, DL488 goat anti-rat 1:750). Hoechst 33342 solution (Thermo Fisher) was used to stain the nuclei. The sections were mounted in Thermo Scientific Fluoromount-G (Thermo Fisher). Sections from all stainings were imaged using a Leica DMLB microscope and a charge-coupled device camera. The analysis and quantification were performed with ImageJ and QuPath,[5] and the average of 3 sections per mouse was taken.

Tissue Lysates

Snap-frozen liver pieces were thawed on ice and lysed in M-PER Mammalian Protein Extraction Reagent (Thermo Fisher Scientific) containing 1% Halt Protease Inhibitor Cocktail (Thermo Fisher Scientific) and 1% Halt Phosphatase Inhibitor Cocktail (Thermo Fisher Scientific). After homogenization with a metal bead in the TissueLyser LT (Qiagen) for 5 minutes at 50 Hz, the lysates were sonicated in a sonicator bath for 5 minutes. Protein amounts were measured using the Nanodrop One Microvolume UV-Vis Spectrophotometer (Thermo Fisher Scientific).

Lipid Analysis

Cholesterol and triglyceride levels of plasma and liver lysates in M-PER buffer (as described above) were measured by using enzymatic assays (Roche diagnostics) according to the manufacturer's protocol.

Alanine-Amino-Transferase/Aspartate Aminotransferase Measurement

Plasma ALT (alanine-amino-transferase) and AST (aspartate aminotransferase) were measured using the VITROS XT 3400 (QuideOrtho), according to the manufacturer's protocol.

ELISA

Inflammatory cytokine levels of liver protein lysates were measured using commercially available ELISA kits from Thermo Fisher Scientific, following the manufacturer's protocol. The concentration of cytokines was normalized to the total protein amount in the tissue lysates.

RNA Sequencing and Analysis

After perfusion with PBS, livers (n=4 for each sex) from *Apoe*$^{-/-}$ *Ahr*$^{-/-}$ and *Apoe*$^{-/-}$ on 12 weeks of high-fat diet were harvested. Tissue samples were collected in RNA-later and snap-frozen in liquid nitrogen. Total RNA was isolated from the samples using the Micro Rneasy kit (Qiagen), according to the manufacturer's protocol. RNA was quantified using RobiGreen, and the RNA quality was checked using the Bioanalyzer platform (RIN value) before library preparation. The average RIN value was 7.0. The libraries were prepared according to standard Illumina protocols and then sequenced by Illumina NovaSeq 6000; Paired-end; sequencing length=150.

FastQC (version 0.11.8) was used to inspect the quality of the raw sequences. All samples pass the quality examination. Adapters were trimmed by TrimGalore (version 0.6.5). Sequencing data were aligned using STAR (version 2.7.8)[6] to the GENCODE referential mouse genome sequence GRCm38.p6 primary assembly version and the GENCODE M25 annotation GTF file. Read counts were quantified using Rsubread (version 2.2.6).[7] Gene differential expression analysis was conducted using the R package DESeq2 (version 1.28.1),[8] controlling sex as a covariate. The parameter alpha in DESeq2 was set to 0.05, and the adjusted $P<0.05$ and the absolute log2-fold change >1 for the significance of differentially expressed genes, followed by gene set overrepresentation analysis based on gene ontology conducted by the R package clusterProfiler (version 4.0.0).[9] For both gene differential expression analysis and gene set overrepresentation analysis, the Benjamini-Hochberg procedure was used for adjusting *P* values. Sequencing data have been deposited in the Gene Expression Omnibus and are publicly available with the accession number GSE173800.

Kinase Activity Profiling

Liver protein lysates (n=3 for each sex) were used for determining STK (serine-threonine kinase) profile by using the PamChip microarray platform with PamStation12 (PamGene International, the Netherlands). To identify phosphorylated Ser/Thr (serine/threonine) for the STK assay, 2.0 µg of protein (n=3 per condition) and 400-µM ATP were applied to each assay along with an STK Basic Mix, consisting of 1× protein PTK (protein tyrosine kinase) reaction buffer, 1× BSA, and 1× STK antibody mix. Before loading the STK Basic Mix onto the arrays, a blocking step was performed using 30 µL of 2% BSA followed by washing with PTK solution for preprocessing. Subsequently, 40 µL of STK Basic Mix was applied to each array. After incubation for an hour (30 °C) where the sample is pumped back and forth through the porous material to maximize binding kinetics and minimize assay time, a fluorescein isothiocyanate–conjugated antibody is used to detect the phosphorylation. Imaging was done using an LED imaging system, and the spot intensity at each time point was quantified (and corrected for local background) using the BioNavigator software version 6.3 (PamGene International, 's-Hertogenbosch, the Netherlands). Overrepresentation analysis of the Gene Ontology, Kyoto Encyclopedia of Genes and Genomes, and WikiPathway database for the kinases with significant differences (median final scores >1.2 and adjusted $P<0.05$) was performed using the R packages clusterProfiler, version 4.8.3.[9] Data were visualized with the R package ggplot2, version 3.4.4.[10]

RNA Analysis, cDNA Synthesis, and qRT-PCR

Liver RNA was isolated using the miRNAeasy kit (Qiagen), following the manufacturer's protocol. cDNA was reverse transcribed using the M-MLV reverse transcriptase (Invitrogen). qRT-PCR was performed with the PowerUp SYBR Green Mastermix (Thermo Fisher Scientific). The following primer pairs were used: β-actin: F: 5'-CAACGAGCGGTTCCGATG-3' and R: 5'-GCCACAGGATTCCATACCCAA-3'; Acot11 (acyl-coenzyme A thioesterase): F: 5'-GGGAGCTCTCCAAGGTGAAG-3' and R: 5'-GTCTTCTCGGCTGGCACCAT-3'; and Usp2 (ubiquitin-specific peptidase): F: 5'-CGCTTCATGGGCTATAATCAGCA-3' and R: 5'-TTCCTCCACATCTGTCGCCC-3'. The qRT-PCR (quantitative reverse transcription polymerase chain reaction) was conducted with the QuantStudio 3 (Thermo Fisher Scientific) PCR system. Melt curves were generated to confirm

specific primer amplification. The relative mRNA expression was calculated using the 2-ddCt method. The reference gene beta-actin was used for normalization.

Flow Cytometry

EDTA-buffered blood was pretreated with erythrocyte lysis buffer (150-mmol/L NH4Cl; 10-mmol/L KHCO3; 0.1-mmol/L diNaEDTA) for 20 minutes. After stopping the reaction with Hank's buffer (Hanks' balanced salt solution, 0.06% 0.5M EDTA, 0.6% BSA, and pH 7.4), the blood was incubated with the following antibody mix: CD45 (APC-Cy7, Invitrogen), Cd115 (fluorescein isothiocyanate, Invitrogen), Gr1 (V500, BioLegend), CD11b (PE-Cy7, Invitrogen), B220 (eF450, Invitrogen), CD3 (PerCP, Invitrogen), CD4 (APC, eBioScience), and CD8 (PE, eBioScience). The flow cytometric analysis was performed with the BD FACS Canto. Cell populations in the blood were gated as follows: total leukocytes (CD45+), monocytes (CD45+CD115+GR1+), neutrophils (CD45+, GR1+), B cells (CD45+CD115-GR1-B220+), and T cells (CD45+CD115-GR1-CD3+). Cell populations and marker expression were analyzed using an FACS CantoTM II with FACS Diva software (BD Biosciences) and analyzed with FlowJo 10.0 (BD Biosciences).

SCENITH

The livers were harvested and smashed with Hank's buffer; first through a 100-µmol/L filter and second through a 40-µmol/L filter. After centrifuging for 5 minutes at 300*g*, the pellet was resuspended in erythrocyte lysis buffer (150-mmol/L NH4Cl, 10-mmol/L KHCO3, and 0.1-mmol/L diNaEDTA) and incubated for 1 minute. After filtering through a 30-µmol/L filter, the pellet was resuspended in 4 mL 40% Percoll (Sigma Aldrich) and slowly layered on top of 4 mL of a 70% Percoll solution. After centrifugation (20 minutes at room temperature, 700*g* without brake), immune cells were collected by taking the distinct interphase, washed twice in PBS, and resuspended in RPMI 1640 with glutamine (Gibco) and supplemented with 10% FCS (Gibco).

The SCENITH (Single Cell EnergetIc Metabolism by Profiling Translation Inhibition) method was performed as described by Arguello et al.[11] The method analyzes protein synthesis by measuring puromycin (puromycin dihydrochloride, Bio-Techne, 10 µg/mL) incorporation with and without the presence of specific metabolic inhibitors. Metabolic pathways blocked were glycolysis and OXPHOS by 2-deoxy-glucose (Sigma Aldrich, 100 mmol/L) and oligomycin (Cell Signaling Technologies, 1 µmol/L), respectively. Homoharringtonine (Sigma Aldrich, 2 µg/mL), a ribosome-targeting drug that blocks protein synthesis, was used as a negative control and background detection. Metabolic requirements and dependencies, that is, glucose dependency, fatty acid and amino acid oxidation, and glycolytic capacity and mitochondrial dependence, were calculated by combining the data of both inhibitors and the net protein biosynthesis. Different immune cells were indicated using the cell surface markers: CD45 (APC-Cy7, BioLegend), CD11b (V500, BD Biosciences), F4/80 (PerCP, BioLegend), NK-1.1 (PB, BioLegend), CD3 (PE, BioLegend), and Ly-6G (PE-Cy7, BioLegend). Intracellular Puromycin was detected using an antipuromycin antibody (AF488, clone 12D10, Sigma Aldrich) in combination with a FOXP3 (forxhead box P3) staining kit (Thermo Fisher).

Analysis of Genetic Association of AHR Variants

We investigated the association between genetic variants in the AHR locus and the prevalence of coronary artery disease in the summary statistics of the latest meta-analysis of the Coronary Artery Disease Genome-Wide Replication and Meta-Analysis plus the Coronary Artery Disease, UK Biobank, and Biobank Japan, cumulatively including 210 842 cases among 1 378 170 participants.[12] We focused on associations at a significance level below the 1% false discovery rate, as defined by $P<2.5\times10^{-5}$.[12,13] We analyzed the association between the lead variant (rs4410790) with lipid traits across the meta-analysis of genome-wide association studies in the cardiovascular and metabolic field (effective sample size >3 000 000), generated by the bottom-line integrative method and accessed via the Common Metabolic Disease and Knowledge Portal (https://hugeamp.org, accessed 2024/11/10).[14] Linkage disequilibrium and recombination rate data were obtained from the International Genome Sample Resource collection.[15] The regional association was visualized with GWASLab (version 3.4.4)[16] using the GRCh37 genome assembly, as in the study by Aragam et al.[12]

Statistics

Statistical analysis was performed using GraphPad Prism 10 (Graphpad Software, Inc). The Gaussian distribution was tested with the Shapiro-Wilk test, and outliers were identified using the ROUT (Robust Regression and Outlier Removal) test. In line with the ARRIVE (Animal Research: Reporting of In Vivo Experiments) guidelines, all animals were included in the analysis, and only statistical outliers were excluded. The unpaired Student 2-tailed *t* test with Welch correction or the Mann-Whitney *U* test was applied to compare 2 groups, as appropriate for data distribution and variance homogeneity. For the weight gain, a 2-way ANOVA with the Bonferroni post hoc tests was used. A 2-tailed $P<0.05$ was considered statistically significant. Data are represented as mean±SEM.

RESULTS

Ahr-Deficient Mice Exhibit a Profound Leukocytosis

Because atherosclerosis is highly associated with systemic inflammation, and the AhR is known to be involved in inflammatory mechanisms, we evaluated leukocyte counts in the blood of mice lacking *Ahr* (*Apoe*$^{-/-}$*Ahr*$^{-/-}$) compared with control mice (*Apoe*$^{-/-}$). As expected, we observed a highly significant leukocytosis in the blood of both male and female *Ahr*-deficient mice. This leukocytosis involved both myeloid (neutrophils and monocytes) and lymphoid (B cells and T cells) cell subsets (Figure 1A). To validate the reproducibility of our findings, we repeated the mouse experiment at another mouse facility, where we observed a similar blood leukocytosis affecting only neutrophils and B and T cells in female mice, while monocytes remained unaffected (Figure S1A). Similarly, significant leukocytosis, with minor sex differences, was observed in the spleens of these mice

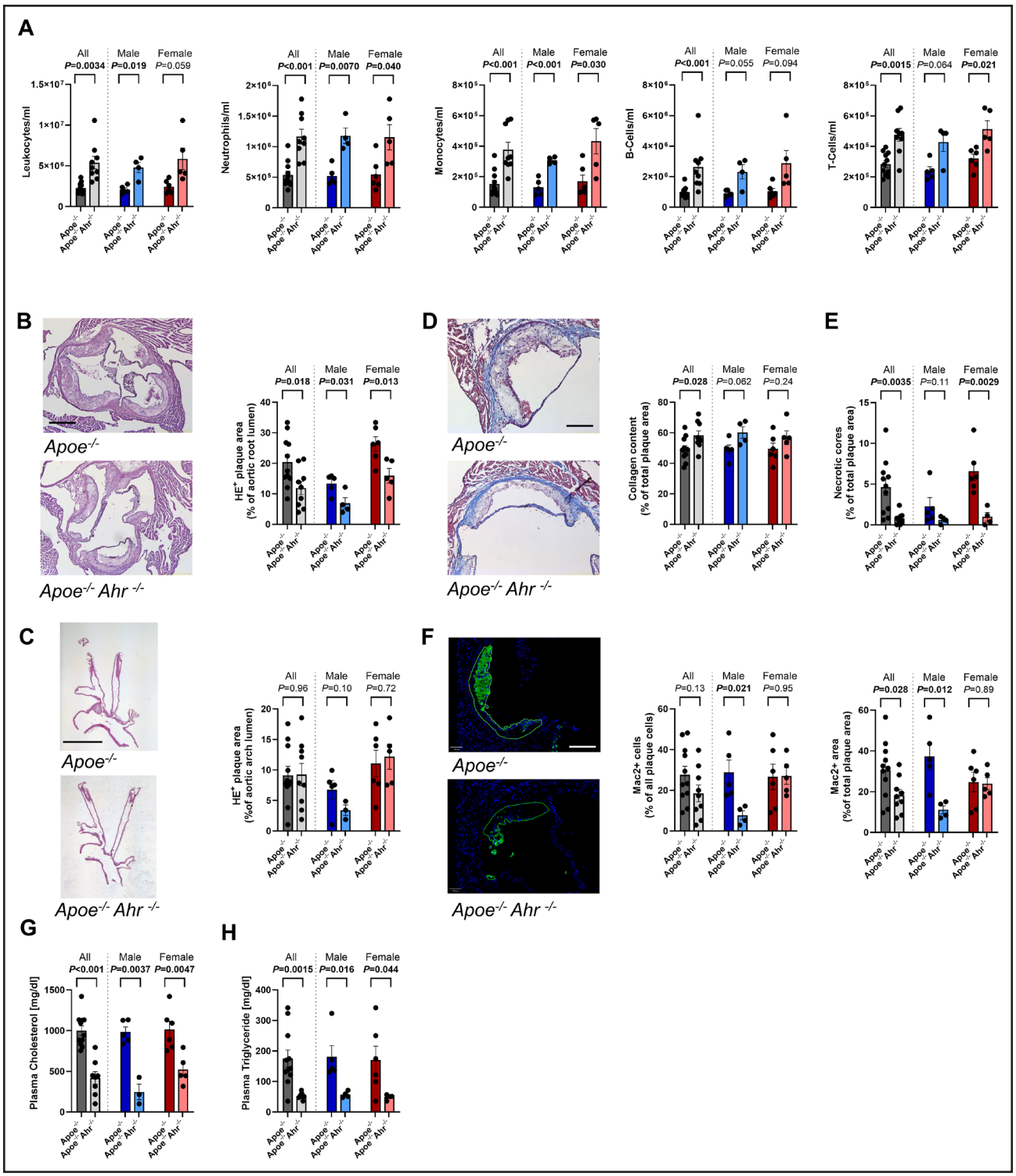

Figure 1. Leukocytosis, though, reduced plaque development in mice lacking *Ahr*.
All results are obtained from *Apoe*$^{-/-}$ and *Apoe*$^{-/-}$*Ahr*$^{-/-}$ mice after 12 weeks of high-fat diet (HFD), with combined sexes, and separated by males and females. **A**, Blood total leukocyte and leukocyte subset counts. **B**, Representative pictures of hematoxylin-eosin–stained aortic roots (scale, 200 µm) with quantification of plaque lesion size. **C**, Representative pictures and quantification of plaque lesion size in aortic arches (scale, 2 mm). **D**, Representative pictures and quantification of collagen content in aortic roots and (**E**) quantification of necrotic cores content. **F**, Representative pictures and quantification of Mac2+ cells. **G**, Plasma cholesterol levels and (**H**) plasma triglyceride levels. Combined n=9 to 11, male n=4 to 6, and female n=4 to 6. Graphs represent mean±SEM.

(Figure S2A and S2B), emphasizing the inflammatory nature of *Ahr* deficiency.

Taken together, we could show in 2 independent experiments that *Ahr* deficiency results in a profound leukocytosis that may exert cardiovascular effects.

Mice Lacking *Ahr* Have Decreased Atherosclerotic Lesion Formation

Given the increased number of circulating leukocytes, we expected that the absence of *Ahr* would lead to greater atherosclerotic lesion formation. However, surprisingly, the plaque size in the aortic roots was significantly decreased in *Apoe*$^{-/-}$*Ahr*$^{-/-}$ mice, with the same effect observed in both male and female mice (Figure 1B; Figure S1B). The plaque size in aortic arches did not change significantly, emphasizing a local effect of the *Ahr* knockout (Figure 1C; Figure S1C). To further characterize the atherosclerotic lesions in the roots, we enumerated macrophages and collagen deposition. The collagen deposition was significantly increased in *Apoe*$^{-/-}$*Ahr*$^{-/-}$ mice compared with *Apoe*$^{-/-}$ mice, while a trend of increased collagen deposition was noticeable in the lesions of male aortic roots, suggesting slightly more stable plaques in one of the independent experiments (Figure 1D; Figure S1D). In line with the smaller plaque size, *Apoe*$^{-/-}$*Ahr*$^{-/-}$ mice also exhibited significantly smaller necrotic cores than control mice (Figure 1E; Figure S1E). The number, as well as the area, of macrophages in the plaques was significantly lower in *Apoe*$^{-/-}$*Ahr*$^{-/-}$ mice although this effect in females was only observed in one of the independent experiments, indicating less inflamed and less progressed plaques (Figure 1F; Figure S1F). While there were no differences in weight gain between the groups in the first experiment, *Apoe*$^{-/-}$*Ahr*$^{-/-}$ mice showed increased body weight gain compared with *Apoe*$^{-/-}$ mice in the second experiment (Figure S3A and S3B). To elucidate possible underlying reasons for the observed reductions in plaque size in this study, we measured plasma cholesterol and triglyceride levels, as hyperlipidemia is another leading risk factor for atherosclerosis. In line with the smaller atherosclerotic lesion sizes, *Apoe*$^{-/-}$*Ahr*$^{-/-}$ mice exhibited significantly lower plasma cholesterol and a striking decrease in triglyceride levels (Figure 1G and 1H; Figure S1G and S1H) in both sexes.

Combined, mice lacking Ahr demonstrate decreased atherosclerotic lesion development despite leukocytosis, suggesting that this is driven by reduced circulating lipid levels.

Altered Hepatic Lipid Metabolism Due to *Ahr* Deficiency

In addition to reduced circulating lipid levels, hepatic lipid levels were significantly decreased in *Apoe*$^{-/-}$*Ahr*$^{-/-}$ mice compared with *Apoe*$^{-/-}$ mice, in both sexes (Figure 2A and 2B), suggesting that the liver plays an essential role in these effects. To understand the changes in lipid levels, we performed RNA sequencing on the livers. Besides the *Cyp*-family regulation, genes not known to be direct AhR targets were also regulated. In particular, genes playing a role in lipid metabolism, such as *Usp2* and *Acot11*, were affected by the lack of *Ahr* (Figure 2C through 2E). Furthermore, Gene Ontology pathway analysis confirmed that differentially expressed genes were involved in several pathways related to cholesterol, fatty acid, and triglyceride metabolism, as well as lipid transfer and storage, highlighting the involvement of the AhR in lipid metabolism (Figure 2F; Figure S4). Focusing in more detail on these pathways, we identified 1 gene, *Apoa4*, which was involved in all 5 upregulated pathways (Figure S5). Interestingly, previous studies have shown that ApoA-IV (apolipoprotein A-IV, the protein encoded by *Apoa4*) reduces hepatic lipid accumulation, primarily by inhibiting lipogenesis,[17–19] which aligns well with our observations.

High hepatic lipid levels often concur with hepatic inflammation. Therefore, we measured the proinflammatory cytokines, TNF (tumor necrosis factor) and CCL2 (CC-chemokine ligand 2), which indeed exhibited a significant decrease in *Ahr*-deficient mice (Figure 2G and 2H). Moreover, we demonstrated that livers from *Ahr*-deficient mice tended to show a less fibrotic phenotype, as evidenced by significantly reduced TGF-β1 levels (Figure S6A), while plasma ALT/AST levels were largely unaffected (Figure S6B).

To gain a more profound understanding of the affected signaling pathways in the liver, we performed an unbiased multiplex kinome activity profiling of the livers. In a combined analysis of males and females (n=6), it was noticeable that a variety of serine-threonine kinases are downregulated in mice lacking the *Ahr*, for example, ARAF (A-Raf proto-oncogene, serine/threonine kinase), BRAF (B-Raf proto-oncogene, serine/threonine kinase), and RAF1 (Raf-1 proto-oncogene, serine/threonine kinase; Figure 2I [significant only]; Figure S7 [complete list]), which are all known to play a role in cell proliferation processes and inflammation.[20] Besides its effect on inflammatory pathways, *Ahr* deficiency also affected liver kinases involved in lipid metabolism, which aligns with our previous observations, as well as kinases involved in glucose metabolism (Table S1). Here, several pathways related to lipid transport are also regulated, suggesting that not only lipogenesis but also lipid transport are affected by AhR. To delve deeper into the effects of AhR on glucose metabolism, as suggested by several other studies,[21] we performed SCENITH on livers from *Apoe*$^{-/-}$*Ahr*$^{-/-}$ and *Apoe*$^{-/-}$ mice. We observed no baseline metabolic differences in Kupffer cells, neutrophils, T cells, or natural cells in *Ahr*-deficient mice (Figure S8A). When comparing the different metabolic pathways, there are also no major differences in immune

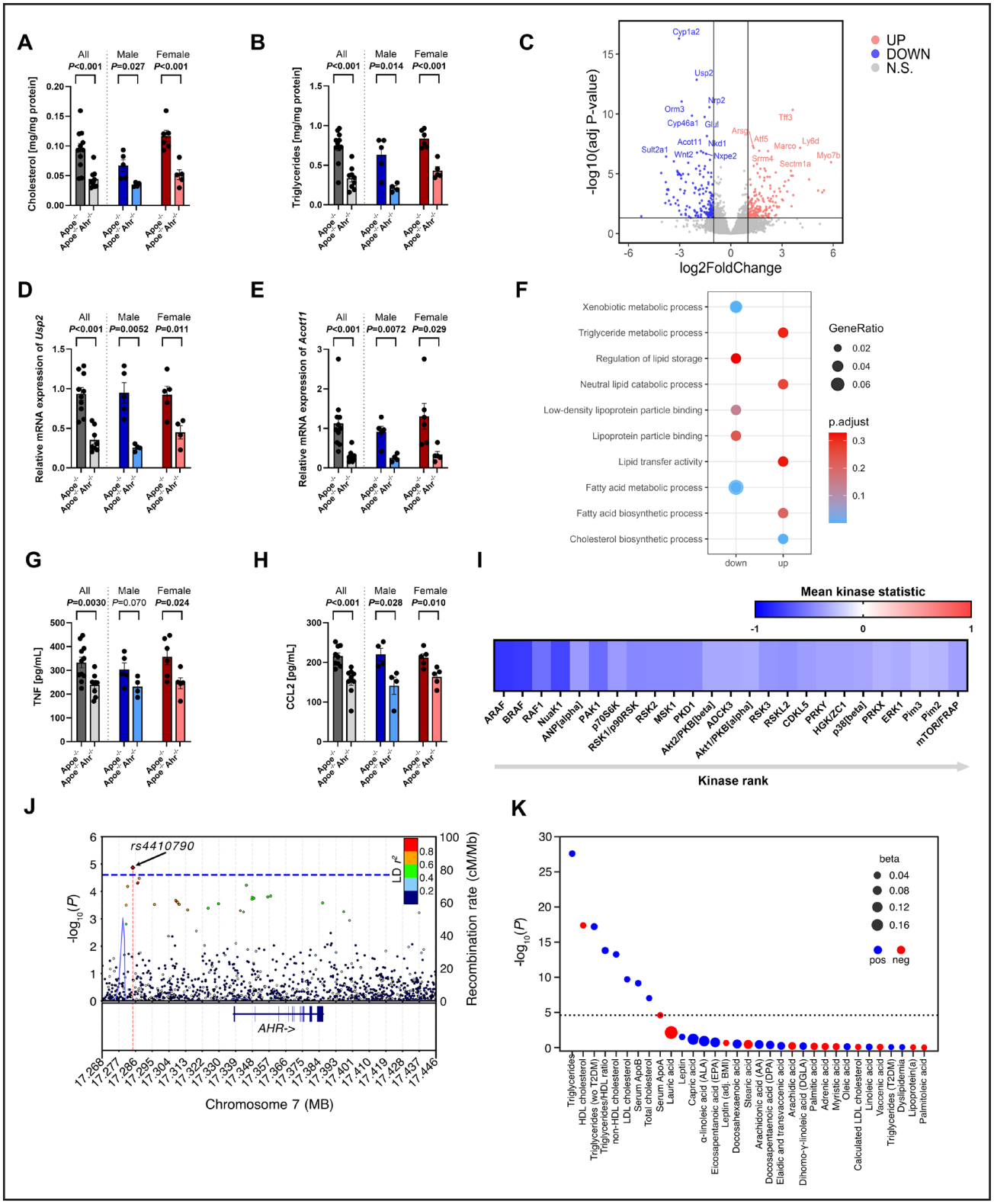

Figure 2. *Ahr* (aryl hydrocarbon receptor) deficiency reduces lipid metabolism and inflammation in the liver.
All mouse results are obtained from *Apoe*$^{-/-}$ and *Apoe*$^{-/-}$*Ahr*$^{-/-}$ mice after 12 weeks of high-fat diet (HFD), with combined sexes, and separated by males and females. **A**, Liver cholesterol and (**B**) liver triglyceride levels. **C**, Volcano plot of liver RNA sequencing–regulated genes, reflecting *Apoe*$^{-/-}$*Ahr*$^{-/-}$ vs *Apoe*$^{-/-}$. **D**, Relative gene expression of *Usp2* and (**E**) *Acot11* in the liver. **F**, Dot plot of Gene Ontology pathway analysis of liver RNA sequencing. **G**, TNF (tumor necrosis factor) and (**H**) CCL2 (CC-chemokine ligand 2) levels in the liver. **I**, Heatmap of significantly regulated STKs (serine-threonine kinases) in the liver. Blue indicates significantly decreased kinase activity in liver tissues of *Apoe*$^{-/-}$*Ahr*$^{-/-}$ vs *Apoe*$^{-/-}$ mice. **J**, Regional association plot of the AHR (aryl hydrocarbon receptor) locus (chr7:17.268.000-17.446.000) based on the meta-analysis of the Coronary Artery Disease Genome-Wide Replication and Meta-Analysis plus the Coronary Artery Disease, (*Continued*)

cells from *Apoe*$^{-/-}$*Ahr*$^{-/-}$ mice compared with cells from *Apoe*$^{-/-}$ mice, except for a small but significant shift in T-cell mitochondrial dependence and glycolytic capacity in males (Figure S8B through S8E). Therefore, although the activity of some metabolism-related kinases was altered, there were no major metabolic changes in hepatic immune cells upon *Ahr* deficiency.

To translate our findings in the mouse model to humans, we analyzed the genetic association between coronary artery disease and genetic variants in the *AHR* locus in a meta-analysis of genome-wide association studies featuring 210 842 cases across 1 378 170 participants.[12] The variant rs4410790 was associated with coronary artery disease for a statistical significance (odds ratio, 0.979 [95% CI, 0.969–0.988]; P=2.26×10^{-5}; Figure 2J) below the 1% false discovery rate threshold, which is in line with coronary artery disease association found for many genes with experimentally proven biological relevance, such as *NPC1L1* (rs41279633; P=1.24×10^{-6}), *PNPLA3* (rs738408; P=1.04×10^{-5}), *MEX3A* (rs11264432; P=3.98×10^{-7}), or *CASR* (rs17251221; P=1.06×10^{-5}).[12,13,22,23] Notably, a PheWAS (Phenome-Wide Association Study) identified significant associations of rs4410790 with lipid traits, including plasma triglyceride (P=2.55×10^{-28}), LDL (low-density lipoprotein; P=1.96×10^{-10}), and total cholesterol (P=9.56×10^{-8}) levels across over 3 million individuals from the genome-wide association study cohorts available in the Common Metabolic Disease and Knowledge Portal (Figure 2K).

Taken together, our data demonstrate that AhR influences hepatic lipid metabolism, which is likely responsible for the observed systemic effects.

DISCUSSION

This study focused on the role of the AhR in atherosclerosis. Due to its known involvement in anti-inflammatory processes, we expected an antiatherosclerotic effect of the AhR. While we indeed observe that *Ahr* deficiency results in leukocytosis, the progression of atherosclerosis was surprisingly reduced in the absence of *Ahr*. While a few other studies have already suggested that the AhR in *Apoe*$^{-/-}$ mice may play a progressive role in atherosclerosis, these studies used pharmacological receptor stimulation, which introduces potential off-target effects, making it difficult to determine the receptor's exact role. For example, Wu et al demonstrated that the activation of AhR in *Apoe*$^{-/-}$ mice by exposure to 2,3,7,8-tetrachlorodibenzo-p-dioxin enhanced atherosclerotic plaque development, mediated by CXCR2 (C-X-C motif chemokine receptor 2) and cholesterol uptake in macrophages,[24] which is in line with our results. A similar study by Bey et al[25] used *Apoe*$^{-/-}$ mice treated with 2,3,7,8-tetrachlorodibenzo-p-dioxin on a standard laboratory diet and confirmed an aggravating effect on atherosclerosis formation, especially in female mice, highlighting sex-specific effects of the AhR. In addition, the well-established interaction between the AhR and estrogen receptor,[26] as well as the generally higher plaque formation in female *Apoe*$^{-/-}$ mice,[27] highlights the differences observed herein between sexes.

In our study, the reduction in atherosclerosis in mice lacking *Ahr* was attributed to decreased plasma lipid levels, which appeared to result from altered liver lipid metabolism. Our results align with multiple mouse studies, in which either genetically induced or ligand-activated AhR activity promoted hepatic lipid accumulation through enhanced fatty acid uptake.[28–30] However, in contrast to our findings, Wada et al[31] showed in a C57BL/6J hepatocyte-specific *Ahr*-knockout mouse model fed a high-fat diet that the lack of *Ahr* increased de novo lipogenesis, with Socs3 (suppressor of cytokine signaling) as the central involved mediator. Mice lacking *Ahr* in hepatocytes additionally exhibited accelerated liver steatosis and fibrosis,[31] whereas we confirmed a rather protective effect of a general *Ahr* knockout on the liver, suggesting that other cell types besides hepatocytes likely also play an essential role in our observed effects. Interestingly, we identified *Apoa4* as a key upregulated gene in *Ahr*-deficient mice, involved in several lipid-related pathways. Several studies have already shown that overexpression of ApoA-IV (the protein encoded by *Apoa4*) in mice results in reduced lipid accumulation in the liver due to decreased lipogenesis, combined with elevated fatty acid β oxidation.[17–19] Another study also already suggested that *Apoa4* is downstream and regulated by the AhR.[32] Therefore, it is interesting to study this potential AhR-ApoA-IV interaction more closely in the future as it might at least partly be the underlying mechanism of our observations.

Regarding hepatic inflammation, the AhR is already known to play a dual role in steatosis models,[33] which differs in part from our findings. Our results indicate that *Ahr* deficiency primarily affects lipid biosynthesis and catabolism but may also affect transport; however, further studies, such as analyzing CD36, an AhR target in some cell types,[29] or applying lipid stainings, are needed to clarify the downstream genes and mechanisms further.

Figure 2 Continued. UK Biobank, and Biobank Japan (1 378 170 individuals).[12] The dashed line delineates the threshold for statistical significance, approximating a false discovery rate (FDR) <1% (P<2.5×10^{-5}). **K**, PheWAS (Phenome-Wide Association Study) for the variant rs4410790 and the lipid traits across the genome-wide association study (GWAS) cohorts included in the Common Metabolic Disease and Knowledge Portal. The dashed line delineates the threshold for statistical significance (FDR <1%). The dot color reflects directionality, while size depicts the β coefficient for each association. Sequencing combined n=6, male n=3, and female n=3; kinomics combined n=6, male n=3 to 5, and female n=3 to 6. Graphs represent mean±SEM.

The differences between those studies and ours may result from divergent cell-cell interactions and, therefore, may be altered differently in a cell-specific mouse model compared with a whole-body *Ahr* knockout. Likewise, a smooth muscle cell-specific *Ahr* deficiency led to larger lesions and altered cap composition, highlighting the context-specific multifaceted role of the AhR and the importance of cell-organ crosstalk.[34] Moreover, the differences might also be due to the *Apoe*$^{-/-}$ background in our study, which affects overall lipid levels, inflammatory processes, and lipoprotein metabolism.[35] Because AhR also plays a role in inflammatory mechanisms and mediates lipid metabolism, mechanisms could counteract lipid metabolism in *Apoe*$^{-/-}$*Ahr*$^{-/-}$ mice, resulting in a mixed inflammatory phenotype. These studies, among others, propose that the role of the AhR in liver lipid metabolism is complex and depends on the ligand, genetic background, and diet of the study animal, making comparisons very challenging and resulting in rather case-dependent outcomes.[36,37]

Initially defined as a cholesterol-driven disorder, atherosclerosis is now recognized to involve inflammation as a central pathogenic mechanism linking diverse risk factors to plaque formation.[38] Interestingly, in our study, blood leukocytes did not affect plaque progression; instead, the overall effect of the AhR on lipid metabolism overruled leukocytosis in mice lacking the AhR on atherosclerotic plaque development. Because high leukocyte levels did not seem to influence plaque development, the functionality of immune cells and endothelial cells may likely be impaired by *Ahr* deficiency. Several studies already confirm the involvement of AhR activation in inflammatory response, cell differentiation, and lipid metabolism of immune cells,[39] which, combined, could alter actions during plaque development.

Because the action of the AhR is ligand- and context-dependent, the results need to be evaluated with caution,[36] especially when considering therapeutic options, as adverse effects may occur depending on ligand specificity. In addition, despite targeting the receptor genetically, it is necessary to further address AhR ligands, such as tryptophan metabolites, which may be altered by a high-fat diet and genetic background. A further limitation of our study is the prior reports, suggesting that *Ahr* deficiency can lead to aberrations in growth and organ development.[40–42] Still, as our mouse model is noninducible, potential embryonic-derived alterations cannot be excluded. Nevertheless, our model, which leverages the receptor's genetic deficiency, offers a sophisticated approach to studying the receptor's role.

CONCLUSIONS AND OUTLOOK

In conclusion, our study demonstrated that the lack of AhR in *Apoe*$^{-/-}$ mice reduces the development of atherosclerotic plaques. It is plausible that this effect originates in the liver, where the absence of Ahr significantly impacts lipid metabolism. This eventually affected plasma lipid levels, which, in turn, influenced lesion size. Despite the high circulating leukocyte levels, lipid metabolism had a dominant impact on plaque development. Our study reveals a major role of the AhR as a lipid mediator in atherosclerotic cardiovascular disease, indicating its potential as a novel therapeutic target.

ARTICLE INFORMATION

Received September 09, 2025; accepted January 9, 2026.

Affiliations

Institute for Molecular Cardiovascular Research, Uniklinik RWTH Aachen (R.H., L.R., A.B.-M., S.L.M., C.M.-P., K.A., J.J., E.A.L.B., E.P.C.v.d.V.), Aachen-Maastricht Institute for Cardio-Renal Disease, Uniklinik RWTH Aachen (R.H., L.R., A.B.-M., S.L.M., C.M.-P., K.A., E.P.C.v.d.V.), Department of Pediatrics (R.J.d.J.), and Department of Internal Medicine I, University Hospital Aachen (E.P.C.v.d.V.), RWTH Aachen University, Germany. Center of Allergy and Environment (ZAUM), Technical University and Helmholtz Center Munich, Germany (R.J.d.J., A.-L.G., C.O.). Central Laboratory, Tianjin Medical University General Hospital, China (H.J.). Department of Pathology, Cardiovascular Research Institute Maastricht, Maastricht UMC, the Netherlands (H.J., J.J., E.A.L.B.). Institute for Cardiovascular Prevention (IPEK), Ludwig-Maximilians-Universität, Munich, Germany (V.T., D.S., E.P.C.v.d.V.). German Centre for Cardiovascular Research (DZHK), Berlin (D.S.). Institute for Genetic and Biomedical Research, Unit of Milan, National Research Council, Italy (D.S.).

Acknowledgments

This work was supported by the Flow Cytometry Facility of the Interdisciplinary Center for Clinical Research (IZKF) within the Faculty of Medicine at RWTH Aachen University.

Sources of Funding

This work was supported by the Corona Foundation (grant S199/10084/2021) to E.P.C. van der Vorst, the Deutsche Forschungsgemeinschaft (grant SFB-TRR219-Project-ID 322900939; subproject M07 to E.P.C. van der Vorst and SFB1123-B05 to D. Santovito), Project-ID OH282/1-2 within FOR2599, Project-ID 490846870–TRR355/1-TPA05 and TPB02, and Project Number 395357507–CRC1371-TP07, the European Research Council (ERC Starting grant, project 716718) to C. Ohnmacht, the BMBF and Free State of Bavaria (LMU Excellence strategy 80325065), grant DZHK-81Z0600203 to D. Santovito, and the Alexander von Humboldt Foundation to R.J. de Jong.

Disclosures

None.

Supplemental Material

Tables S1–S2
Figures S1–S8
Major Resources Table

REFERENCES

1. Libby P. The changing landscape of atherosclerosis. *Nature*. 2021;592:524–533. doi: 10.1038/s41586-021-03392-8
2. Kou Z, Dai W. Aryl hydrocarbon receptor: its roles in physiology. *Biochem Pharmacol*. 2021;185:114428. doi: 10.1016/j.bcp.2021.114428
3. Natividad JM, Agus A, Planchais J, Lamas B, Jarry AC, Martin R, Michel ML, Chong-Nguyen C, Roussel R, Straube M, et al. Impaired Aryl hydrocarbon receptor ligand production by the gut microbiota is a key factor in metabolic syndrome. *Cell Metab*. 2018;28:737–749.e4. doi: 10.1016/j.cmet.2018.07.001
4. Zhu K, Meng Q, Zhang Z, Yi T, He Y, Zheng J, Lei W. Aryl hydrocarbon receptor pathway: role, regulation and intervention in atherosclerosis therapy (Review). *Mol Med Rep*. 2019;20:4763–4773. doi: 10.3892/mmr.2019.10748
5. Bankhead P, Loughrey MB, Fernandez JA, Dombrowski Y, McArt DG, Dunne PD, McQuaid S, Gray RT, Murray LJ, Coleman HG, et al.

QuPath: Open source software for digital pathology image analysis. *Sci Rep*. 2017;7:16878. doi: 10.1038/s41598-017-17204-5
6. Dobin A, Davis CA, Schlesinger F, Drenkow J, Zaleski C, Jha S, Batut P, Chaisson M, Gingeras TR. STAR: ultrafast universal RNA-seq aligner. *Bioinformatics*. 2012;29:15–21. doi: 10.1093/bioinformatics/bts635
7. Liao Y, Smyth GK, Shi W. The R package Rsubread is easier, faster, cheaper and better for alignment and quantification of RNA sequencing reads. *Nucleic Acids Res*. 2019;47:e47–e47. doi: 10.1093/nar/gkz114
8. Love MI, Huber W, Anders S. Moderated estimation of fold change and dispersion for RNA-seq data with DESeq2. *Genome Biol*. 2014;15:550. doi: 10.1186/s13059-014-0550-8
9. Wu T, Hu E, Xu S, Chen M, Guo P, Dai Z, Feng T, Zhou L, Tang W, Zhan L, et al. clusterProfiler 4.0: A universal enrichment tool for interpreting omics data. *Innovation (Camb)*. 2021;2:100141. doi: 10.1016/j.xinn.2021.100141
10. Wickham H. *ggplot2: elegant graphics for data analysis*. Springer International Publishing; 2016.
11. Arguello RJ, Combes AJ, Char R, Gigan JP, Baaziz AI, Bousiquot E, Camosseto V, Samad B, Tsui J, Yan P, et al. SCENITH: a flow cytometry-based method to functionally profile energy metabolism with single-cell resolution. *Cell Metab*. 2020;32:1063–1075.e7. doi: 10.1016/j.cmet.2020.11.007
12. Aragam KG, Jiang T, Goel A, Kanoni S, Wolford BN, Atri DS, Weeks EM, Wang M, Hindy G, Zhou W, et al; Biobank Japan. Discovery and systematic characterization of risk variants and genes for coronary artery disease in over a million participants. *Nat Genet*. 2022;54:1803–1815. doi: 10.1038/s41588-022-01233-6
13. Santovito D, Henderson JM, Bidzhekov K, Triantafyllidou V, Jansen Y, Chen Z, Farina FM, Diagel A, Aslani M, Blanchet X, et al. Mex3a protects against atherosclerosis: evidence from mice and humans. *Circulation*. 2024;150:1213–1216. doi: 10.1161/CIRCULATIONAHA.124.069526
14. Pulit SL, Stoneman C, Morris AP, Wood AR, Glastonbury CA, Tyrrell J, Yengo L, Ferreira T, Marouli E, Ji Y, et al; GIANT Consortium. Meta-analysis of genome-wide association studies for body fat distribution in 694 649 individuals of European ancestry. *Hum Mol Genet*. 2019;28:166–174. doi: 10.1093/hmg/ddy327
15. Fairley S, Lowy-Gallego E, Perry E, Flicek P. The International Genome Sample Resource (IGSR) collection of open human genomic variation resources. *Nucleic Acids Res*. 2020;48:D941–D947. doi: 10.1093/nar/gkz836
16. He Y, Koido M, Shimmori Y, Kamatani Y. GWASLab: a Python package for processing and visualizing GWAS summary statistics. *Preprint Jxiv*. 2023. doi: 10.51094/jxiv.370
17. Cheng C, Liu XH, He J, Gao J, Zhou JT, Fan JN, Jin X, Zhang J, Chang L, Xiong Z, et al. Apolipoprotein A4 restricts diet-induced hepatic steatosis via SREBF1-mediated lipogenesis and enhances IRS-PI3K-Akt signaling. *Mol Nutr Food Res*. 2022;66:e2101034. doi: 10.1002/mnfr.202101034
18. VerHague MA, Cheng D, Weinberg RB, Shelness GS. Apolipoprotein A-IV expression in mouse liver enhances triglyceride secretion and reduces hepatic lipid content by promoting very low density lipoprotein particle expansion. *Arterioscler Thromb Vasc Biol*. 2013;33:2501–2508. doi: 10.1161/ATVBAHA.113.301948
19. Lundsgaard AM, Del Giudice R, Kanta JM, Larance M, Armour SL, London A, Richter MM, Andersen NR, Nicolaisen TS, Carl CS, et al. Apolipoprotein A-IV is induced by high-fat diets and mediates positive effects on glucose and lipid metabolism. *Mol Metab*. 2025;95:102119. doi: 10.1016/j.molmet.2025.102119
20. Ullah R, Yin Q, Snell AH, Wan L. RAF-MEK-ERK pathway in cancer evolution and treatment. *Semin Cancer Biol*. 2022;85:123–154. doi: 10.1016/j.semcancer.2021.05.010
21. Sayed TS, Maayah ZH, Zeidan HA, Agouni A, Korashy HM. Insight into the physiological and pathological roles of the aryl hydrocarbon receptor pathway in glucose homeostasis, insulin resistance, and diabetes development. *Cell Mol Biol Lett*. 2022;27:103. doi: 10.1186/s11658-022-00397-7
22. Adam S, Maas SL, Huchzermeier R, Rakateli L, Abschlag K, Hohl M, Liao L, Bartneck M, Teunissen M, Wouters K, et al. The calcium-sensing-receptor (CaSR) in adipocytes contributes to sex-differences in the susceptibility to high fat diet induced obesity and atherosclerosis. *EBioMedicine*. 2024;107:105293. doi: 10.1016/j.ebiom.2024.105293
23. Romeo S, Kozlitina J, Xing C, Pertsemlidis A, Cox D, Pennacchio LA, Boerwinkle E, Cohen JC, Hobbs HH. Genetic variation in PNPLA3 confers susceptibility to nonalcoholic fatty liver disease. *Nat Genet*. 2008;40:1461–1465. doi: 10.1038/ng.257
24. Wu D, Nishimura N, Kuo V, Fiehn O, Shahbaz S, Van Winkle L, Matsumura F, Vogel CF. Activation of aryl hydrocarbon receptor induces vascular inflammation and promotes atherosclerosis in apolipoprotein E-/- mice. *Arterioscler Thromb Vasc Biol*. 2011;31:1260–1267. doi: 10.1161/ATVBAHA.110.220202
25. Bey L, Coumoul X, Kim MJ. TCDD aggravates the formation of the atherosclerotic plaque in ApoE KO mice with a sexual dimorphic pattern. *Biochimie*. 2022;195:54–58. doi: 10.1016/j.biochi.2022.01.012
26. Tarnow P, Tralau T, Luch A. Chemical activation of estrogen and aryl hydrocarbon receptor signaling pathways and their interaction in toxicology and metabolism. *Expert Opin Drug Metab Toxicol*. 2019;15:219–229. doi: 10.1080/17425255.2019.1569627
27. Christ C, Ocskay Z, Kovacs G, Jakus Z. Characterization of atherosclerotic mice reveals a sex-dependent susceptibility to plaque calcification but no major changes in the lymphatics in the arterial wall. *Int J Mol Sci*. 2024;25:4046. doi: 10.3390/ijms25074046
28. Kawano Y, Nishiumi S, Tanaka S, Nobutani K, Miki A, Yano Y, Seo Y, Kutsumi H, Ashida H, Azuma T, et al. Activation of the aryl hydrocarbon receptor induces hepatic steatosis via the upregulation of fatty acid transport. *Arch Biochem Biophys*. 2010;504:221–227. doi: 10.1016/j.abb.2010.09.001
29. Lee JH, Wada T, Febbraio M, He J, Matsubara T, Lee MJ, Gonzalez FJ, Xie W. A novel role for the dioxin receptor in fatty acid metabolism and hepatic steatosis. *Gastroenterology*. 2010;139:653–663. doi: 10.1053/j.gastro.2010.03.033
30. Sambrook PN, Champion GD, Browne CD, Cairns D, Cohen ML, Day RO, Graham S, Handel M, Jaworski R, Kempler S. Corticosteroid injection for osteoarthritis of the knee: peripatellar compared to intra-articular route. *Clin Exp Rheumatol*. 1989;7:609–613.
31. Wada T, Sunaga H, Miyata K, Shirasaki H, Uchiyama Y, Shimba S. Aryl hydrocarbon receptor plays protective roles against high fat diet (HFD)-induced hepatic steatosis and the subsequent lipotoxicity via direct transcriptional regulation of Socs3 gene expression. *J Biol Chem*. 2016;291:7004–7016. doi: 10.1074/jbc.M115.693655
32. Kerley-Hamilton JS, Trask HW, Ridley CJ, Dufour E, Ringelberg CS, Nurinova N, Wong D, Moodie KL, Shipman SL, Moore JH, et al. Obesity is mediated by differential aryl hydrocarbon receptor signaling in mice fed a Western diet. *Environ Health Perspect*. 2012;120:1252–1259. doi: 10.1289/ehp.1205003
33. Xu CX, Wang C, Zhang ZM, Jaeger CD, Krager SL, Bottum KM, Liu J, Liao DF, Tischkau SA. Aryl hydrocarbon receptor deficiency protects mice from diet-induced adiposity and metabolic disorders through increased energy expenditure. *Int J Obes (Lond)*. 2015;39:1300–1309. doi: 10.1038/ijo.2015.63
34. Kim JB, Zhao Q, Nguyen T, Pjanic M, Cheng P, Wirka R, Travisano S, Nagao M, Kundu R, Quertermous T. Environment-sensing aryl hydrocarbon receptor inhibits the chondrogenic fate of modulated smooth muscle cells in atherosclerotic lesions. *Circulation*. 2020;142:575–590. doi: 10.1161/CIRCULATIONAHA.120.045981
35. Oppi S, Luscher TF, Stein S. Mouse models for atherosclerosis research-which is my line? *Front Cardiovasc Med*. 2019;6:46. doi: 10.3389/fcvm.2019.00046
36. Jurgelewicz A, Dornbos P, Warren M, Nault R, Arkatkar A, Lin H, Threadgill DW, Zacharewski T, LaPres JJ. Genetics-based approach to identify novel genes regulated by the aryl hydrocarbon receptor in mouse liver. *Toxicol Sci*. 2021;181:285–294. doi: 10.1093/toxsci/kfab032
37. Jin J, Wahlang B, Thapa M, Head KZ, Hardesty JE, Srivastava S, Merchant ML, Rai SN, Prough RA, Cave MC. Proteomics and metabolic phenotyping define principal roles for the aryl hydrocarbon receptor in mouse liver. *Acta Pharm Sin B*. 2021;11:3806–3819. doi: 10.1016/j.apsb.2021.10.014
38. Libby P. Inflammation in atherosclerosis. *Arterioscler Thromb Vasc Biol*. 2012;32:2045–2051. doi: 10.1161/ATVBAHA.108.179705
39. Maier AM, Huth K, Alessandrini F, Schnautz B, Arifovic A, Riols F, Haid M, Koegler A, Sameith K, Schmidt-Weber CB, et al. The aryl hydrocarbon receptor regulates lipid mediator production in alveolar macrophages. *Front Immunol*. 2023;14:1157373. doi: 10.3389/fimmu.2023.1157373
40. Fernandez-Salguero P, Pineau T, Hilbert DM, McPhail T, Lee SS, Kimura S, Nebert DW, Rudikoff S, Ward JM, Gonzalez FJ. Immune system impairment and hepatic fibrosis in mice lacking the dioxin-binding Ah receptor. *Science*. 1995;268:722–726. doi: 10.1126/science.7732381
41. Fernandez-Salguero PM, Ward JM, Sundberg JP, Gonzalez FJ. Lesions of aryl-hydrocarbon receptor-deficient mice. *Vet Pathol*. 1997;34:605–614. doi: 10.1177/030098589703400609
42. Lahvis GP, Lindell SL, Thomas RS, McCuskey RS, Murphy C, Glover E, Bentz M, Southard J, Bradfield CA. Portosystemic shunting and persistent fetal vascular structures in aryl hydrocarbon receptor-deficient mice. *Proc Natl Acad Sci USA*. 2000;97:10442–10447. doi: 10.1073/pnas.190256997